Applied Catalysis B: Environmental 91 (2009) 619–627

Contents lists available at ScienceDirect

Applied Catalysis B: Environmental

journal homepage: www.elsevier.com/locate/apcatb

Photocatalytic behavior of TOPO-capped TiO_2 nanocrystals for degradation of endocrine disrupting chemicals

Sue-min Chang *, Pin-han Lo, Chen-tuan Chang

Institute of Environmental Engineering, National Chiao Tung University, 1001, University Road, Hsinchu 30010, Taiwan

ARTICLE INFO

Article history:
Received 11 March 2009
Received in revised form 23 June 2009
Accepted 30 June 2009
Available online 8 July 2009

Keywords:
Ligand-capped TiO_2
Endocrine disrupting chemicals
Photocatalytic degradation

ABSTRACT

In this study, we investigated the photocatalytic kinetics and mechanisms of trioctylphosphine oxide-capped titanium dioxide (TOPO-capped TiO_2) for degradation of two endocrine disrupting chemicals (EDCs), phenol and bisphenol A, which contained different hydrophobicity, chemiadsorbability, and degradable capacity. The TOPO-capped TiO_2 exhibited high partition coefficients of 2.00×10^{-4} and 3.42×10^{-3} l/mg for phenol and bisphenol A, respectively. In addition, the bonded TOPO introduced substantial amounts of trapped holes at the surface. The high affinity toward the target compounds and stabilized charge carriers resulted in high photocatalytic activity of the modified TiO_2. The TOPO-capped TiO_2 exhibited 12- and 3-fold higher photocatalytic activities than P25 for decomposition of bisphenol A and phenol, respectively. The presence of the hydrophobic modifier inhibited the generation of hydroxyl radicals and led to the photocatalysis undergoing mainly from partition followed by chemisorption and interfacial charge transfer. Partition and interfacial charge transfer were the rate determining steps for the degradation of phenol and bisphenol A, respectively. According to the Langmuir–Hinshelwood model, the adsorption coefficient (K_a) and intrinsic rate constant (k_r) for phenol were 4.17×10^{-2} l/mg and 5.60×10^{-2} mg-g/l-min-m^2, respectively, while they were 2.91×10^{-2} l/m and 2.18×10^{-1} mg-g/l-min-m^2, respectively for bisphenol A degradation. The product of the k_r and K_a for bisphenol A was 2.7 times higher than that for phenol, revealing that the modified TiO_2 favored decomposition of the compound which contains high chemiadsorbability and direct photocatalytic tendency in their individual systems. In contrast, the high degradable capability of phenol resulted in its preferential degradation in the competitive system.

1. Introduction

Endocrine disrupting chemicals (EDCs) have attracted great concern nowadays because they mimic hormonal activity and interfere with the functions of endocrine systems [1]. Several adverse effects such as spontaneous abortion, neutron-behavioral disorder, skewed sex rations within the offspring of the exposed communities, intersex, impaired immune function, and varieties of cancers are induced by EDCs. Some of the effects have been found in ecosystem and potentially take place on human health in the future [2]. The leakage of EDCs to the environment is mainly from industrial, agricultural and sewage runoff. High hydrophobicity of EDCs results in their great accumulation in activated sludge during bio-transformation or biodegradation, thereby significantly decreasing the treatment efficiency. Titanium dioxide (TiO_2)-based photocatalysis has been demonstrated to effectively decompose EDCs within a short reaction period [3,4]. In addition, the high chemical stability and UV-sensitive property of TiO_2 cause the photocatalysis as the promising technique for sustainable and environmental friendly treatments.

Photocatalysis is initiated through photo-activation of TiO_2 which induces electron transitions from valence to conduction band and form electron–hole pairs. Afterwards, diffusion and interfacial transfer of the charge carriers to the adsorbed reactants on the surface of TiO_2 result in oxidized or reduced reactions [5]. High photocatalytic activity is the result of inhibited charge recombination, enhanced charge transfer and improved adsorbability toward target compounds. Microstructures and surface compositions of TiO_2 control these behaviors [6,7]. Anatase TiO_2 generally exhibits better photocatalytic performance than rutile phase because defects in the anatase lattice trap charges and retard recombination [8]. Size-controlled photocatalytic activity is associated with available reactive sites and charge diffusion length [9]. Small sizes increase the surface areas to maximize interfacial charge transfer. In addition, the reduced scales decrease charge diffusion length, thus minimizing volume charge recombination.

Surface characteristics dominate the acidity, hydrophobicity and surface electronic properties of TiO_2, thereby influencing its

* Corresponding author. Tel.: +886 3 5712121x55506.
E-mail address: chang@mail.nctu.edu.tw (S.-m. Chang).

0926-3373/$ – see front matter © 2009 Elsevier B.V. All rights reserved.
doi:10.1016/j.apcatb.2009.06.035

adsorptions, kinetics and mechanisms of photocatalytic reactions [7,10,11]. Surface modification with organic compounds has been demonstrated to enhance photocatalytic activity of TiO_2 via improving surface affinity toward reactants and interfacial charge transfer [12–14]. Li et al. modified TiO_2 with 5-sulfosalicylic acid and enhanced greatly its adsorption efficiency toward nitrophenol from 42 to 84%. Correspondingly, this effect doubled the photocatalytic activity of the modified TiO_2 under a certain condition. Mele et al. [15] impregnated TiO_2 with porphyrin and found enhanced photocatalytic performance for degradation of 4-nitrophenol. This enhancement was due to that porphyrin attracted delocalized charge carriers and prolonged charge lifetime for efficient charge transfer to water or O_2.

The improved extent on the photocatalytic activity of modified TiO_2 is dependent on intrinsic natures of target compounds. Park and Choi [16] reported that Nafion changed the surface charges of TiO_2 from positive to negative and increased the adsorptions of positively charged dye by electrostatic interaction. This effect largely enhanced the degradation efficiency of the cationic dye on the surface of the modified TiO_2. However, the decomposition of anionic dye was only slightly improved even though the charge recombination was inhibited by the Nafion. Cropek et al. [17] reported that arginine-modified TiO_2 selectively reduced nitrobenzene but had negligible degradation for phenol. This selectivity was resulted from the improved attractions between the electron-deficient nitrobenzene and electron-rich arginine. In contrast, the weak coupling effect between phenol and the surface modifier prevented its adsorption and photocatalytic oxidation. Previously, we prepared TiO_2 anatase nanocrystals using a non-hydrolytic sol–gel method (NHSG) when trioctylphosphine oxide (TOPO) was used as a capping agent [18]. The TOPO was chemically bonded to the surface of TiO_2 in terms of formation of Ti–O–P bonds or chelation of the P=O groups to Ti^{4+} centers. The TOPO-capped TiO_2 exhibited 1.7 times higher photocatalytic activity than Degussa P25 for degradation of rhodamine B. However, its photocatalytic behavior for degradation of EDCs is unclear.

In this study, we further investigated the photocatalytic behaviors of the TOPO-capped TiO_2 for degradation of two EDCs including phenol and bisphenol A. The effects of the surface modifier and microstructures of the TOPO-capped TiO_2 on the photocatalytic kinetics and mechanisms were understood through examination of dark adsorptions, trapped charges, and photogenerated hydroxyl radicals. To determine the key features dominating the photocatalytic behaviors for the compounds, all the degradation rates and physicochemical properties of the surface modified TiO_2 were referenced to those of P25. Moreover, the preferential activities for certain compounds in the individual and competitive systems were elucidated based on the hydrophobicity, chemiadsorbability and degradable capability of the target chemicals.

2. Experimental

2.1. Preparation of TOPO-capped TiO_2

Surface modified TiO_2 nanocrystals were prepared by cross-condensation between $TiCl_4$ (Showa, 99.9%) and $Ti(OC_3H_7)_4$ (Acros organics, 98%) in the presence of TOPO (Strem chemicals, 99%) using a non-hydrolytic sol–gel manner. The $TiCl_4$ (0.47 g, 2.5 mmol) and $Ti(OC_3H_7)_4$ (0.71 g, 2.5 mmol) were dissolved in molten TOPO (5.22 g, 13.5 mmol) at 150 °C under N_2 atmosphere with vigorous stirring at 500 rpm for 15 min. The temperature was then increased to 400 °C to induce cross-condensation of $TiCl_4$ and $Ti(OC_3H_7)_4$ at this temperature for 3 h. Afterwards, the solution was cooled down to 60 °C followed by adding acetone for precipitation of nano-particles. The precipitate was harvested by centrifugation at 11,000 rpm for 10 min and washed with acetone several times to remove excess TOPO. After drying, the precipitate was grinded to fine powders.

2.2. Characterization

The microstructures of the TiO_2 nano-particles were examined using a high resolution transmission electron microscopy (HRTEM, JEOL JEM-2010) at an accelerating voltage of 200 kV. The crystalline properties of the samples were indentified by an X-ray diffractometer (XRD, Rigaku) using Cu Kα radiation (λ = 1.5405 Å) and operating at an accelerating voltage of 30 kV and an emission current of 20 mA. The diffraction patterns were recorded from 20 to 90° 2θ position at a sampling rate of 4° min^{-1} and a sampling width of 0.02°. Nitrogen adsorptions were measured at 77 K using a N_2 adsorption analyzer (Micromeritics ASAP 2020). The surface areas of the TiO_2 were estimated using the Brunauer–Emmett–Teller (BET) model according to the N_2 adsorption data. The surface compositions were characterized by an X-ray photoelectron spectrometer (XPS, Physical Electronics, ESCA PHI 1600) using an Al Kα radiation (1486.6 eV). The weight fraction of the organic moiety to the total mass of the TiO_2 was determined using a thermal gravimeter (Netzsch, TG 209 F1) operated under an air flow of 20 ml/min and at a heating rate of 10 °C/min from 20 to 900 °C. The functional groups were indentified using a Fourier transform infrared spectrometer (FTIR Horiba FT-720) scanning from 400 to 4000 cm^{-1} with a resolution of 4 cm^{-1} for 100 runs. The optical property of the TiO_2 nano-particles was detected by an UV–vis spectrometer (Hitachi 3010) equipped with an integrating sphere (60 mm DIA) and using Al_2O_3 as a reference. A diffuse-reflectance spectrum was recorded from 800 to 200 nm and then converted to absorption coefficients using Kubelka–Munk theory.

2.3. Electron paramagnetic resonance (EPR) measurement

The EPR measurements were carried out using a Bruker EMX spectrometer working at X-band frequency. A 500 W Xe lamp (Ushio Inc.) with major output wavelength at 365 nm was equipped to the sample cavity by lined optical fiber. The spectra of trapped charges in the photocatalysts were recorded at room temperature or 77 K in the dark or with illumination. Photogenerated hydroxyl radicals were measured by spin trapping method. Oxygen-saturated TiO_2 suspensions (1 g/l) containing 5,5-dimethyl-1-pyrroline N-oxide (DMPO, Aldrich, 2.7×10^{-3} M) were irradiated with UV light at room temperature. The instrumental conditions were set at a center field of 3400–3510 G and a sweep width of 200.0 G. The microwave frequency was 9.49–9.88 GHz with a power at 8.02 mV.

2.4. Sorption behavior

Batch sorption equilibriums were conducted in the dark at room temperature using 8 ml PTFE-lined screw cap glass vials. Suspensions were prepared by mixing the EDCs solutions (5 ml) of various concentrations with TiO_2 under vigorous stirring. The dosage of TiO_2 in each batch test was maintained at 1 g/l. After adsorption, the slurry was centrifuged at 15,000 rpm for 3 min to remove the photocatalysts. The remaining amounts of EDCs in the supernatant were analyzed using a high-performance liquid chromatograph (HPLC, Waters Alliance 2695) equipped with a photodiode array detector (PDA, Waters 2996) and a C18 column (5 μm, 4.6 mm × 250 mm). The mobile phases for phenol and bisphenol A were methanol–water (50/50, v/v) and acetonitrile–water (50/50, v/v) mixtures, respectively, at a constant flow rate of 1.0 ml/min. Adsorption equilibrium time was studied by a parallel approach. Adsorbed amounts of the EDCs were measured after mixing for different periods of time. The equilibriums were

achieved within 10 min. Thus, adsorption isotherms were examined after mixing for 30 min to ensure equilibrium.

2.5. Photocatalytic degradation

The photocatalytic degradation was carried out in a quartz water-jacked reactor sounded by 8 W UV-lamps with major irradiation at 305 nm. The EDCs were firstly dissolved in O_2-saturated water to prepare stock solutions of 100 mg/l. Then, the stock solutions were diluted into various concentrations (10–50 mg/l) for followed photocatalysis. Prior photocatalytic degradation, TOPO-capped TiO_2 was added into the EDCs solutions with vigorous stirring for 30 min in the dark to reach adsorption equilibrium. After illumination, the slurry was sampled at different time intervals followed by centrifugation for removal of photocatalysts. The changes in the concentrations of EDCs were determined by HPLC.

3. Results and discussion

3.1. Characteristics of TOPO-capped TiO_2

The TOPO-capped TiO_2 nanocrystals were prepared through a NHSG method. Detailed properties of the NHSG-derived TiO_2 have been addressed in our previous paper [18]. The TEM image shows that the TiO_2 exhibited spherical shape and had a diameter of ca. 5 nm (see Supplementary Material, Fig. S1). In addition, each particle contained highly single crystallinity. Anatase phase with an average size of 4.9 nm were determined from its XRD pattern (see Supplementary Material, Fig. S2). The UV absorption edge of the TiO_2 was at 349.2 nm, corresponding to a band gap of 3.6 eV. This band gap was larger than that of bulk anatase TiO_2 (3.2 eV), indicating the quantum size effect. The FTIR spectra show the stretching modes of alky chains and P–O at 2800–3000 and 1085 cm^{-1}, respectively, revealing the TOPO was chemically bound to the surface of TiO_2 through formation of P–O–Ti bonds. (see Supplementary Material, Fig. S3). The TGA curve of the sample indicates that the hydrocarbons of TOPO contribute 15% to total mass of the TOPO-capped TiO_2 (see Supplementary Material, Fig. S4). The specific surface area of the TOPO-capped TiO_2 was 7.00 m^2/g. This value was significantly less than the theoretical one (706 m^2/g) which was calculated from its diameter (5.0 nm) and density (1.7 g/cm^3). This discrepancy is mainly due to strong hydrophobic interaction between the TOPO-capped nanocrystals which leads to serious aggregations. The C/P ratio of the modified TiO_2 determined using XPS was 13.2. This value was smaller than the stoichiometric one (C/P = 24) of TOPO, indicating that alky chains of the modifier underwent partially thermal decomposition during the NHSG process at high temperature.

3.2. Sorption behavior

To understand the effects of the adsorption ability of the TOPO-capped TiO_2 on its photocatalytic activities, we examined the dark adsorption isotherms for the target compounds in the same concentration ranges used for the following photocatalytic tests. Fig. 1 shows the sorption isotherms of phenol and bisphenol A with initial concentrations of 10–50 mg/l in the presence of TOPO-capped TiO_2 or P25. The adsorbed amounts (q, mg/g) of the EDCs were linearly dependent on their equilibrium concentrations in the TOPO-capped TiO_2 suspensions. This correlation clearly reveals that the binding mechanism of the EDCs on the TOPO-capped TiO_2 mainly based on non-specific hydrophobic interaction. We obtained their partition coefficients (K) from the regression of the linear range between q and C_e. The K values of phenol and bisphenol A between water and the surface TOPO were 2.00×10^{-4} and 3.42×10^{-3} l/mg, respectively. These values were positively correlated to their log K_{ow} which are 1.5 and 3.2 for phenol and bisphenol A, respectively [19,20]. Therefore, the TOPO-capped TiO_2 had higher capacity for enrichment of more hydrophobic organic compounds on its surface. On the other hand, the adsorption amounts of phenol and bisphenol A on P25 ranged 0.24–0.42 mg/g. Since these values were close to their detection limits (0.22 mg/g for phenol, and 0.26 mg/g for bisphenol A), P25 showed negligible adsorptions toward these EDCs.

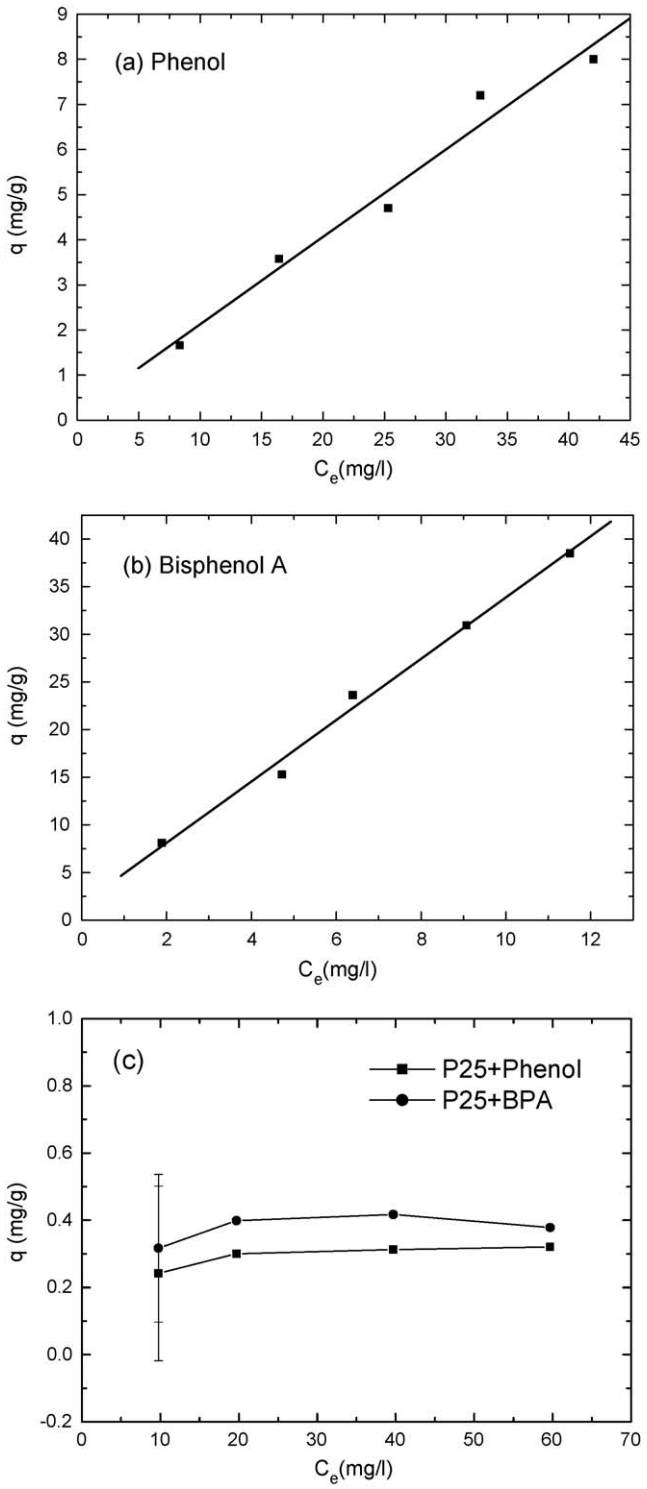

Fig. 1. Sorption isotherm of (a) phenol and (b) bisphenol A in the TOPO-capped TiO_2 suspensions and (c) the EDCs in the presence of P25.

3.3. EPR measurement

Fig. 2 shows the EPR spectra of TOPO-capped TiO_2 and P25 acquired in the dark or under UV illumination at room temperature. The irradiated P25 exhibited two sets of g values: one with $g_1 = 2.011$, $g_2 = 2.008$, $g_3 = 2.002$ and the other with $g_1 = 2.028$, $g_2 = 2.018$, $g_3 = 2.006$. The former set of g values labeled as signal A is assigned to surface ozonide ions $Ti^{4+}O_3^-$. This species is formed when O_2 participate charge carrier trapping processes [21]. The latter is ascribed to a surface hole trapped radical $Ti^{4+}O^{2-}Ti^{4+}O^-$ and is presented as signal B [22]. Prior to UV irradiation, the P25 had already shown the weak signals of $Ti^{4+}O_3^-$ and $Ti^{4+}O^{2-}Ti^{4+}O^-$. Since the samples were not preheated and degassed in the dark, the stabilized trapping holes are presumably due to the removal of electrons by adsorbed oxygen [23]. The TOPO-capped TiO_2 showed different types of hole-trapping from P25. Without UV irradiation, the TOPO-capped TiO_2 showed a set of g values at $g_1 = 2.025$ and $g_3 = 2.005$ which are labeled as signal C. We attribute the intensive signal C to $Ti^{4+}O^{\bullet-}OP\text{-}R_3$. The Ti–O–P bonds were formed by deformation of the P=O group of TOPO during non-hydrolytic sol–gel synthesis. The existence of $Ti^{4+}O^{\bullet-}OP\text{-}R_3$ before illumination indicates that the unoccupied P^{5+} energy levels were close to those of O anions. Thus, the electron transition from O^{2-} to P^{5+} states was accessible by thermal excitation at room temperature. Irradiation with UV induced surface hydroxyl trapped hole signals $Ti^{4+}O^{\bullet-}Ti^{4+}OH^-$ at $g_1 = 2.018$, $g_2 = 2.011$ and $g_3 = 2.002$, which are presented as signal D. Weak signals with the lines at $g_1 = 2.035$, $g_2 = 2.009$ and $g_3 = 2.002$ are ascribed to $Ti^{4+}O_2H^\bullet$ and are displayed as signal E. This radical was generated from electron trapping by O_2 followed by proton capture [21]. Signals D and E indicate dissociative chemisorption of water on the surface of the TOPO-capped TiO_2. However, such hyroxylated signals were not obvious in the irradiated P25 sample.

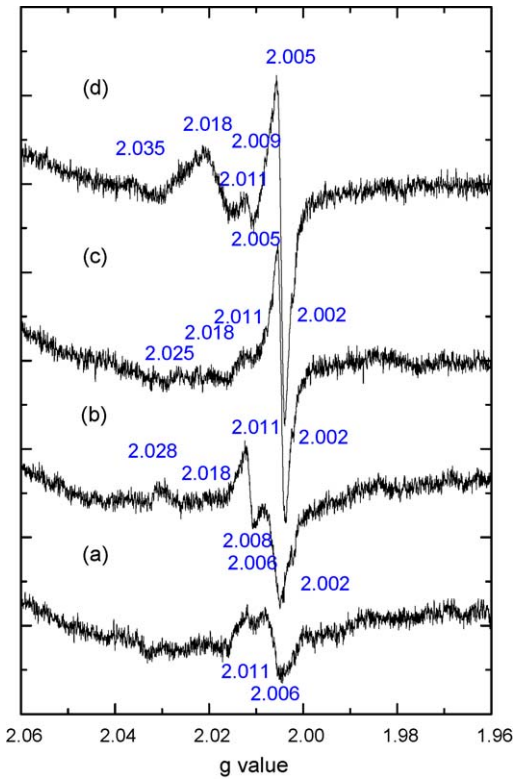

Fig. 2. The EPR spectra of (a) non-irradiated P25, (b) irradiated P25, (c) non-irradiated TOPO-capped TiO_2, and (d) irradiated TOPO-capped TiO_2. All the spectra were measured at room temperature.

We attribute this discrepancy to that the $Ti^{4+}O^{\bullet-}OP\text{-}R_3$ radicals possess more reductive potential than the $Ti^{4+}O^{2-}Ti^{4+}O^-$ to induce the donation of electrons from water because the unoccupied 3d states of P^{5+} ions are located at the lower energy range of the valence band of TiO_2 [24]. In addition, the TOPO-capped TiO_2 provided substantial amounts of the hole trapping sites at the surface. The trapped holes help the chemisorption not only of water but also substrates, thus improving photocatalytic activity [25]. The peak-to-peak heights of the first derivative EPR signals are adapted for quantification of the trapping sites. The difference in the intensities of signals before and after illumination refers to the capability of the photocatalysts for charge stabilization. The TOPO-capped TiO_2 exhibited a population of trapped photogenerated holes which was 3.4 times higher than that of P25. Most of the holes (76%) in the modified TiO_2 were trapped by surface bonded TOPO. The parameters of the different signals assigned to the oxygenated species, along with the literature values, are collected in Table 1.

Fig. 3 shows the EPR spectra of the photocatalysts acquired before or after UV illumination at 77 K. Hole trapping signals (signals A, D and E) in the TOPO-capped TiO_2 and P25 became broad and weak because of limited amounts of vapor and oxygen in the sealed sample cells. In addition, low temperature inhibited the $O \rightarrow P$ electron transition and reduced the intensity of the $Ti^{4+}O^{\bullet-}OP\text{-}R_3$ signal in the TOPO-capped TiO_2 in the dark. After irradiation with UV, the modified TiO_2 showed intensive signals at $g_\perp = 1.991$ and $g_\parallel = 1.961$ which were arose from inner lattice trapped Ti^{3+} sites and are labeled as signal F. Table 2 lists the parameters of the Ti^{3+} sites in the anatase TiO_2 in the present study and those from literature results. However, the signal F was not detected in the illuminated P25, indicating the prompt recombination of electron–hole pairs. The prolonged lifetime of the photogenerated electrons in the TOPO-capped TiO_2 was attributed to discrete unoccupied levels in the quantum sized crystals (5 nm) which served as trapping centers for stabilization of the charges. A weak signal at $g = 1.979$ corresponding to four-coordinated Ti^{3+} centers was also observed in the irradiated TOPO-capped TiO_2 and is assigned as signal G [6]. Similar peaks are generally detected in the interface between silica and titania coatings or between anatase and rutile phases [6,26]. In this study, the unsaturated Ti^{4+} ions were resulted from the incorporation of TOPO in the surface lattice of the TiO_2 that sterically hindered the formation of Ti–O bonds during synthesis. They located mainly at the surface of the TiO_2 nanocrystals.

Semiconductor-based photocatalysis involves two pathways. One is the generation of hydroxyl radicals followed by attack of the OH radicals to organic pollutants for decomposition. The other is

Table 1
EPR parameters of the oxygen related signals in the anatase TiO_2 along with the literature values measured for similar species.

System/assignment	g-Tensors			Ref.
	g_1	g_2	g_3	
$Ti^{4+}O_3^-$ (signal A)	2.011	2.008	2.002	[a]
	2.011	2.007	2.002	[21]
$Ti^{4+}O^{2-}Ti^{4+}O^-$ (signal B)	2.028	2.018	2.006	[a]
	2.026	2.015	2.005	[23]
$Ti^{4+}O^{\bullet-}OP\text{-}R_3$ (signal C)	2.025	–	2.005	[a]
	2.023	–	2.004	[21]
$Ti^{4+}O^{\bullet-}Ti^{4+}OH^-$ (signal D)	2.018	2.011	2.002	[a]
	2.016	2.012	2.002	[23]
$Ti^{4+}O_2H^\bullet$ (signal E)	2.035	2.009	2.002	[a]
	2.034	2.009	2.002	[21]

[a] This work.

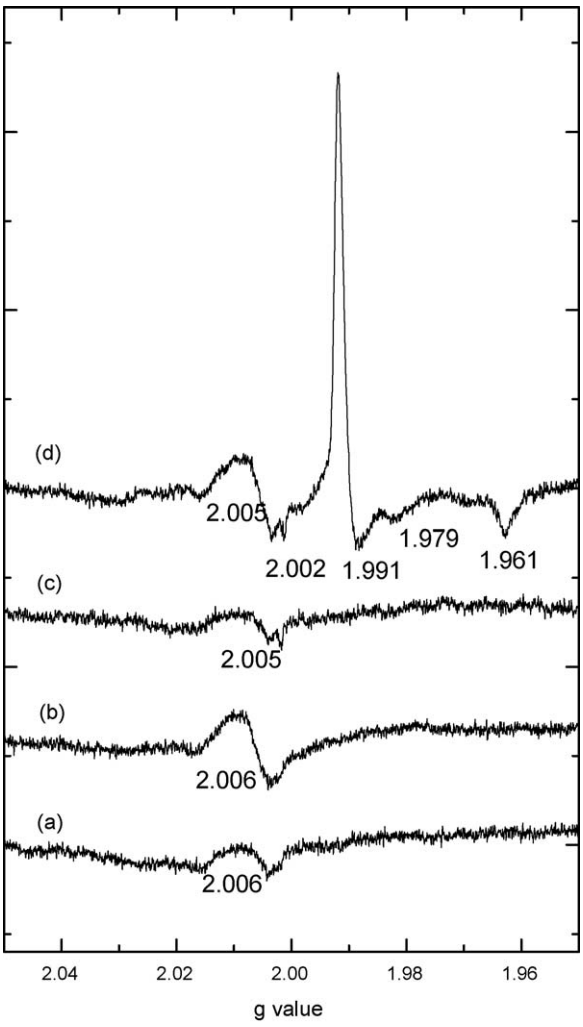

Fig. 3. The EPR spectra measured at 77 K for (a) non-irradiated P25, (b) irradiated P25, (c) non-irradiated TOPO-capped TiO_2, and (d) irradiated TOPO-capped TiO_2.

direct reaction of the organic pollutants with charge carriers trapped in the surface layer of TiO_2. To understand the mechanism occurring on the TOPO-capped TiO_2, we determine the generation of photocatalytic induced OH radicals using DMPO as a spin-trap agent. Fig. 4 shows the EPR spectra of DMPO spin adducts in the solutions containing TOPO-capped TiO_2 or P25 both at 1 mg/l under illumination of UV light at room temperature. The P25 suspension clearly displayed the characteristic 1:2:2:1 quartet of DMPO-OH• spin adducts. However, the generation of the spin adducts was insignificant in the TOPO-capped TiO_2 suspension under the same irradiation. We normalized the signals with surface areas of the photocatalysts and found that the intensity of the spin adducts in the P25 suspension still showed 9 times higher than that in the TOPO-capped TiO_2 slurry. Hydroxyl radicals are

Table 2
EPR parameters of the Ti^{3+} sites in the anatase TiO_2 along with the literature values measured for similar species.

System/assignment	g-Tensors		Ref.
	$g_\perp$	$g_\parallel$	
Inner Ti^{3+} sites (signal F)	1.991	1.961	[a]
	1.990	1.960	[21]
Four-coordinated Ti^{3+} (signal G)	1.979		[a], [6]

[a] This work.

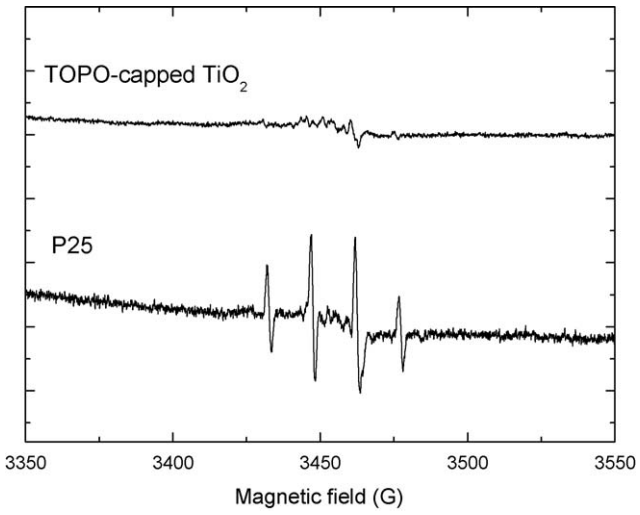

Fig. 4. EPR spectra of DMPO-OH• spin adducts in the P25 and TOPO-capped TiO_2 suspensions under illumination.

mainly produced by donation of electrons from adsorbed water or OH anions to the surface trapped holes. The high intensity of the DMPO-OH• spin adducts in the P25 suspension indicates that the degradation of organic pollutants upon the un-modified TiO_2 was mainly induced by attack of radicals. As to the TOPO modified TiO_2, the hydrophobic character of the organic modifier prevented the adsorption of water on the TiO_2. Therefore, the decomposition of organic compounds in the TOPO-capped TiO_2 systems was basically initiated by direct photocatalysis.

3.4. Photocatalytic degradation of EDCs

Fig. 5 shows the degradation of 10 ppm phenol and bisphenol A in the presence of TOPO-capped TiO_2 and P25 at 1 g/l. The TOPO-capped TiO_2 remarkably reduced 15% of phenol and 81% of bisohenol A in the initial 30 min sorption equilibrium in the dark via partition. Photocatalysis by the modified TiO_2 further reached 98% removal efficiency for phenol in 180 min and 95% removal efficiency for bisphenol A in 90 min illumination. Dark adsorptions of phenol and bisphenol A by P25 were not obvious. P25 decomposed 98% of phenol and 93% of bisphenol A in 90 and 240 min illumination, respectively.

The kinetics of photocatalysis is generally described using the Langmuir–Hinshelwood (L–H) model which can be expressed as follows:

$$r = \frac{k_r K_a C}{1 + K_a C} \quad (1)$$

where r is an initial decomposition rate (mg/l-min), k_r (mg/l-min) means an intrinsic rate constant, K_a (l/mg) represents adsorption coefficient, and C (mg/l) is the concentration of a reactant under an equilibrium condition. The model states that the surface reactions occur after sorption equilibriums. The photocatalysis by the TOPO-capped TiO_2 mainly involves with physisorption of reactants (R) in the modifier layer (step 1) followed by chemisorption of the reactants to the bare TiO_2 surface (step 2) for direct photocatalytic degradation (step 3). The three elemental steps can be expressed as following equations:"

$$R + TOPO - TiO_2 \leftrightarrow R\,TOPO - TiO_2 \quad (2)$$

$$R\,TOPO - TiO_2 \leftrightarrow R - TiO_2 - TOPO \quad (3)$$

$$R - TiO_2 - TOPO \rightarrow P - TiO_2 - TOPO \quad (4)$$

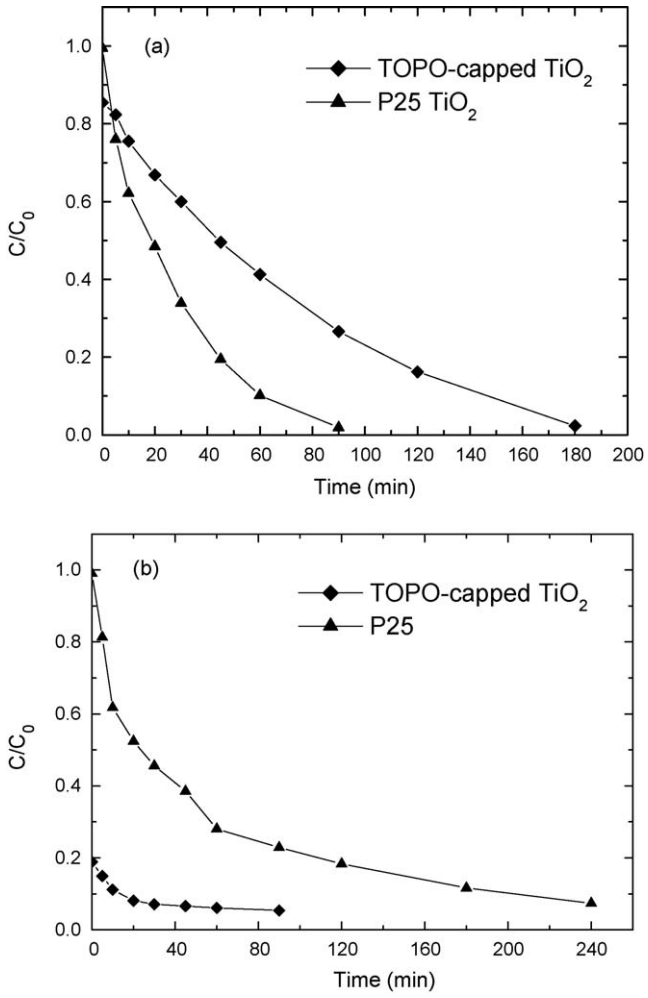

Fig. 5. The photocatalytic degradation of (a) phenol and (b) bisphenol A with initial concentrations of 10 mg/l in the presence of P25 (▲) and TOPO-capped TiO_2 (◆).

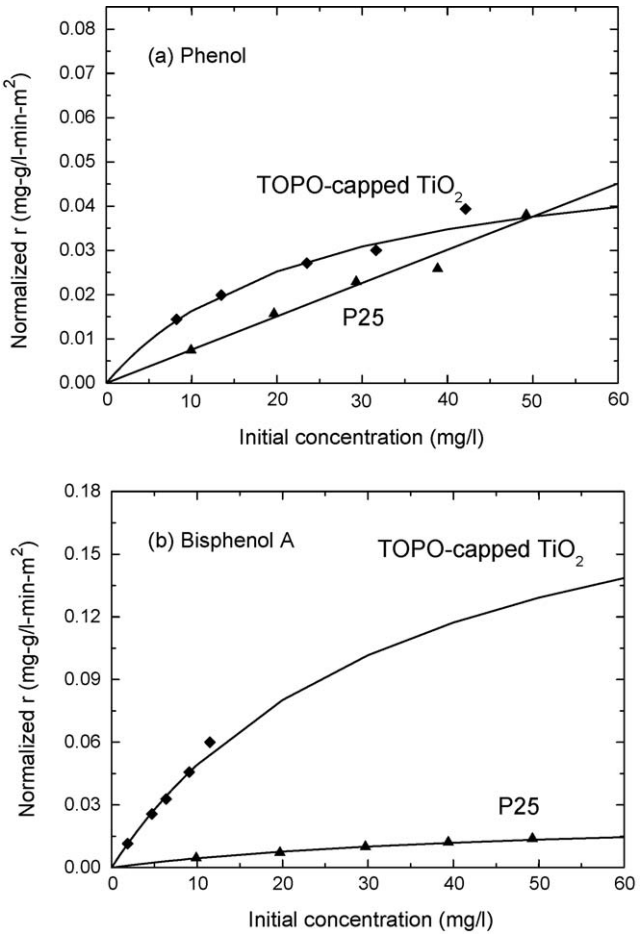

Fig. 6. The dependence of normalized initial decomposition rate on different initial concentrations of (a) phenol and (b) bisphenol A in the P25 (▲) and TOPO-capped TiO_2 (◆) suspensions. The solid lines represent the model results according to Langmuir–Hinshelwood kinetics.

where P represents products. According to Eq. (1), decomposition rates positively correlate with concentrations. However, the TOPO-capped TiO_2 exhibited a lag in the degradation of phenol within first 5 min illumination. This phenomenon suggests that partition of phenol to the TOPO layer (step 1) was relatively slower than its chemisorption. Thus, the partition was the rate determining step of the photocatalysis in the beginning. The partition rate increased upon the decreasing concentrations of the adsorbed phenol in the TOPO layer by the prompt surface reaction. In the meantime, the surface reaction slowed down because of inefficient partition and chemisorption. The partition and surface reaction rates gradually approached to a kinetic equilibrium after 5 min illumination. After that, the removal rates of phenol in the solutions corresponded to photocatalytic degradation rates. We took this condition as the initial state to study the photocatalytic kinetics of phenol using the L–H model. In contrast, the degradation of bisphenol A by the TOPO-capped TiO_2 fitted the L–H model when the UV was turned on. This phenomenon suggests that partition of bisphenol A to the TOPO layer was either faster or equal to its chemisorption rate. Thus, the removal rate of bisphenol A from the solution almost corresponded to its photocatalytic degradation rate.

Fig. 6 shows the experimental and model dependence of the specific initial degradation rates of the target compounds against their different initial concentrations in the presence of TOPO-capped TiO_2 and P25. The TOPO-capped TiO_2 performed higher degradation rates than P25 for both phenol and bisphenol A. The decomposition rates of phenol by TOPO-capped TiO_2 were 1.44×10^{-2}–3.93×10^{-2} mg-g/l-min-m^2 at initial concentration of 8.2–42.1 mg/l. P25 decomposed phenol by the initial rates of 7.44×10^{-3}–3.80×10^{-2} mg-g/l-min-m^2 at 9.94–49.23 mg/l. The L–H model depicted that the modified TiO_2 exhibited 3-fold higher activity than P25 at maximum. However, the improvement declined with increasing initial concentrations. The TOPO-capped TiO_2 lost the superiority on the photocatalytic activity when the initial concentration was over 50 mg/l. On the other hand, partition effect of TOPO-capped TiO_2 greatly decreased the initial concentrations of bisphenol A from 10–50 to 1.89–11.51 mg/l. In addition, the degradation rates of bisphenol A by the modified TiO_2 were 1.14×10^{-2}–6.00×10^{-2} mg-g/l-min-m^2 at these low initial concentrations. P25 showed the degradation rates of 4.51×10^{-3}–1.38×10^{-2} mg-g/l-min-m^2 at 9.90–49.25 mg/l. The L–H model inferred that the modified TiO_2 performed 11.7-fold improvement at most on the photocatalytic activity relative to P25. Moreover, the improvement only slightly declined 20% with increasing concentrations up to 60 mg/l. The high photoactivity of the TOPO-capped TiO_2 was mainly contributed by its high partition coefficients and lots of stabilized charges which effectively improved compound diffusion from bulk solution to the surface and facilitated interfacial charge transfer [13,27,28]. Comparelli et al. [29] compared the photodegradation efficiency of azo dyes in the presence of TOPO-capped TiO_2 to that in the P25 suspensions. They reported, however, that the organic-capped TiO_2 exhibited lower degradation rates than the commercial product although the organic modifier assisted to concentrate the dyes onto the TiO_2

surface. The lack of terminated hydroxyl groups and prohibited adsorption of water on the surface were considered to cause the detrimental effects. We attribute this discrepancy to different microscopic mechanisms induced by different chemical structures of target compounds. To clarify the compound dependent mechanisms and kinetics, we determined the adsorption coefficients and intrinsic rate constants of phenol and bisphenol A according to the transformed L–H model:

$$\frac{1}{r} = \frac{1}{k_r} + \frac{1}{k_r K_a} \times \frac{1}{C} \quad (5)$$

The k_r and K_a were estimated from the intercept and slope of the linear fit of $1/r$ versus $1/C$, respectively, and were summarized in Table 3. The TOPO-capped TiO_2 exhibited a K_a of 4.17×10^{-2} l/mg for phenol. Since partition rate of phenol was comparatively lower than its chemisorption rate, the K_a represented mainly the physiadsorbaility of the modified TiO_2 toward this compound. The adsorption coefficient of phenol determined under irradiation was 209 times larger than its partition coefficient measured in the dark (2.00×10^{-4} l/mg). The difference was resulted from photoinduced changes in the surface electronic structures [30]. Compared to the K_a measured in the P25 suspension (9.84×10^{-5} l/mg), the K_a of the modified TiO_2 was 424 times higher. The intrinsic rate constant of the TOPO-capped TiO_2 for the degradation of phenol was 5.60×10^{-2} mg-g/l-min-m^2. In contrast, this constant was 137 times lower than that determined on P25 (7.69 mg-g/l-min-m^2). The small K_a of the un-modified TiO_2 (P25) suggests that the degradation of phenol was primarily mediated by hydroxyl radicals. However, the generation of hydroxyl radicals was inhibited by the presence of the surface organic modifier, thereby reducing the surface reactivity of the TOPO-capped TiO_2. Effective partition compensated the detrimental effects and dominated the improved photocatalytic activity of the modified TiO_2 at low concentrations of phenol. However, this advantage diminished upon the increasing concentrations while surface reactivity in turn governed the photocatalytic activity.

The k_r and K_a of TOPO-capped TiO_2 for degradation of bisphenol A were 2.18×10^{-1} mg-g/l-min-m^2 and 2.91×10^{-2} l/mg, respectively. The K_a for this case represents the chemiadsorbability of bisphenol A on the modified TiO_2 because its partition was efficient during photocatalysis. P25 showed the k_r and K_a of 2.65×10^{-2} mg-g/l-min-m^2 and 2.04×10^{-2} l/mg, respectively. In contrast to phenol, P25 exhibited high K_a for bisphenol A, suggesting that this compound tended to be decomposed through direct photocatalysis because of its high chemiadsorbability. It is noted that the k_r and K_a of TOPO-capped TiO_2 were 8.5- and 1.5-fold higher than those of P25. We attribute the improved chemisorptions on the modified TiO_2 to larger amounts of surface trapped holes. The strong chemisorptions can facilitate interfacial charge transfer, thereby enhancing its surface reactivity [11]. Moreover, the TiO_2 nanocrystals stabilized more electrons and provided shorter charge diffusion length than P25, also resulting in the high surface reactivity. The model results showed that the TOPO-capped TiO_2 exhibited the superior activity for degradation of bisphenol A over a wide concentration range. This merit is as the result of combined contributions from improved adsorption and surface reactivity. Ooka et al. [31] studied the photocatalytic activity of TiO_2 for the degradation of the EDCs having different hydrophobicity. They reported that adsorptions controlled the activity, and the compounds having larger K_{ow} values exhibited higher adsorption constants and reaction rate constants. In our study, the products of k_r and K_a of the TOPO-capped TiO_2 for phenol and bisphenol A were 2.34×10^{-3} and 6.34×10^{-3} g/min-m^2, respectively. The higher product for bisphenol A indicates that TOPO-capped TiO_2 favors decomposing the compound which has high chemiadsorption ability and mainly underwent direct photocatalysis.

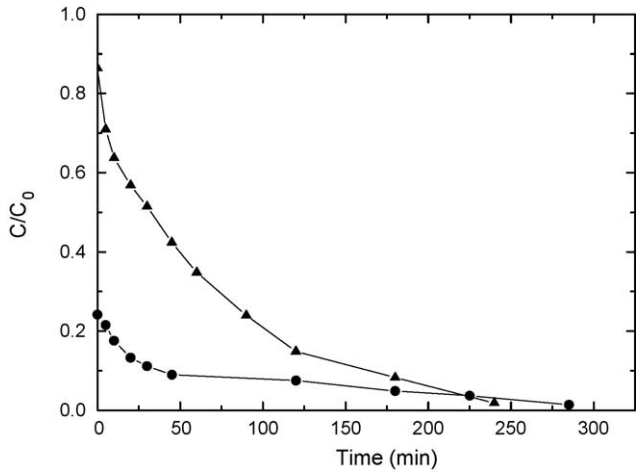

Fig. 7. The photodegradation of (▲) phenol and (●) bisphenol A by TOPO-capped TiO_2 in the competitive system.

To understand whether the TOPO-capped TiO_2 still selectively decomposes bisphenol A in the presence of phenol, a competitive photocatalysis was carried out. Fig. 7 shows the degradation curves of phenol and bisphenol A with both initial concentrations of 10 mg/l in the competitive system. Partition effect initially decreased the concentrations of phenol and bisphenol A from 10 mg/l to 8.6 and 2.4 mg/l, respectively. The final concentrations in the competitive system were similar to those in their individual ones, indicating insignificant competition on partition. However, the lagged removal of phenol which was found in the beginning of its photocatalysis in the individual system disappeared in the mixed solution. This phenomenon suggests that the degradation rate of phenol was enhanced by the presence of bisphenol A. The initial degradation rates of phenol and bisphenol A were 3.23×10^{-2} and 9.43×10^{-3} mg-g/l-min-m^2, respectively. Compared to those measured in their individual systems, the mixed solution remarkably promoted 2.5-fold increase in the degradation rate for phenol but slightly decreased the decomposition rate for bisphenol A. The improved degradation of phenol was presumably due to the increased amounts of radicals in the TOPO layer. These radicals were generated through the direct interaction of bisphenol A with surface trapped holes. However, the direct photocatalysis of bisphenol A was hindered by competitive chemiadsorption of phenol. The competitive system removed 98 and 95% of phenol and bisphenol A after 240 and 285 min illumination, respectively. These periods were 1.3- and 3.2-fold longer, respectively, than

Table 3
Intrinsic rate constants (k_r) and adsorption coefficients (K_a) of phenol and bisphenol A in the TOPO-capped TiO_2 and P25 suspensions.

	Phenol			Bisphenol A		
	k_r (mg-g/l-min-m^2)	K_a (l/mg)	R^2	k_r (mg-g/l-min-m^2)	K_a (l/mg)	R^2
TOPO-capped TiO_2	5.60×10^{-2}	4.17×10^{-2}	0.990	2.18×10^{-1}	2.91×10^{-2}	0.998
P25 TiO_2	7.69	9.84×10^{-5}	0.995	2.65×10^{-2}	2.04×10^{-2}	0.991

those required for the same removal efficiency in their individual systems. The prolonged degradation was resulted from the limited active sites for the increased amounts of reactants. Compared to bisphenol A, the higher initial degradation rate (3.23×10^{-2} mg-g/l-min-m^2) and the shorter decomposition time (240 min) for phenol indicate that the TOPO-capped TiO_2 preferentially decomposed the compound with higher intrinsic degradable capability in the competitive system. Actually, in the individual systems, the k_r for phenol (7.69 mg-g/l-min-m^2) was 290 times higher than that for bisphenol A (2.65×10^{-2} mg-g/l-min-m^2) on the P25. The high surface reactivity for phenol supports our deduction.

3.5. Surface properties of the used photocatalysts

To understand the stability of the surface organic modifier during photocatalysis, we examined the surface functional groups and chemical compositions of the used TOPO-capped TiO_2 after photocatalytic tests. Fig. 8 shows the FTIR spectra of the used TOPO-capped TiO_2 after first and second photocatalytic degradation of 10 ppm phenol and bisphenol A. After one photocatalytic run, the used samples still showed intensive C–H (2800–3000 cm^{-1}) and P–O stretching absorptions (1108 cm^{-1}). The XPS results indicated that the C/P ratio of the modified TiO_2 decreased from 13.2 to 7.9–8.6, while its P/Ti still remained the similar value of 0.4–0.5. The decreased C/P ratio reveals the decomposition of the organic moiety of TOPO. To verify whether the decomposition is resulted from direct photocatalysis or photogenerated radicals, we further determined the chemical compositions of the TOPO-capped TiO_2 irradiated in the vacuum and in the aerated water for 2 h. In contrast to the used photocatalysts, these two samples exhibited similar C/P (13.8–17.4) and P/Ti (0.4) ratios to those of as-prepared TOPO-capped TiO_2. These findings indicate that the chemically bonded TOPO had high stability against direct photocatalysis. However, the radicals generated by the interaction of the EDCs or O_2 with trapped charge carriers decomposed the alky chains of the modifier. It is noted that washing the used photocatalysts with acetone decreased their P/Ti ratios to 0.3 after first photocatalytic runs. Moreover, either the intensities of C–H or P–O stretching absorptions were decreased in their FTIR spectra. These phenomena indicate that the Ti–O^1–P–O^2 covalent bonds underwent transformation during photocatalysis and turned the strongly bonded TOPO to be weakly bound to the TiO_2 upon hydrogen bonding, van der Waal's interaction or P═O → Ti^{4+} chelating. According to the EPR spectrum of the irradiated TOPO-capped TiO_2 in air (Fig. 2d), this transformation presumably involves with the Ti–O^1 and P–O^2 bond breaking and reformation of P═O bonds that take place via O^1 → P electron transition followed by attacking of the Ti ions with electron acceptors, O_2. Blue-shift of the P–O stretching absorption from 1085 to 1108 cm^{-1} after photocatalysis also supports the dissociation of the bonded TOPO from the TiO_2 surface. Repeated photocatalysis caused more amounts of TOPO detached. The C–H or P–O stretching absorptions were almost diminished in the secondly recovered photocatalysts.

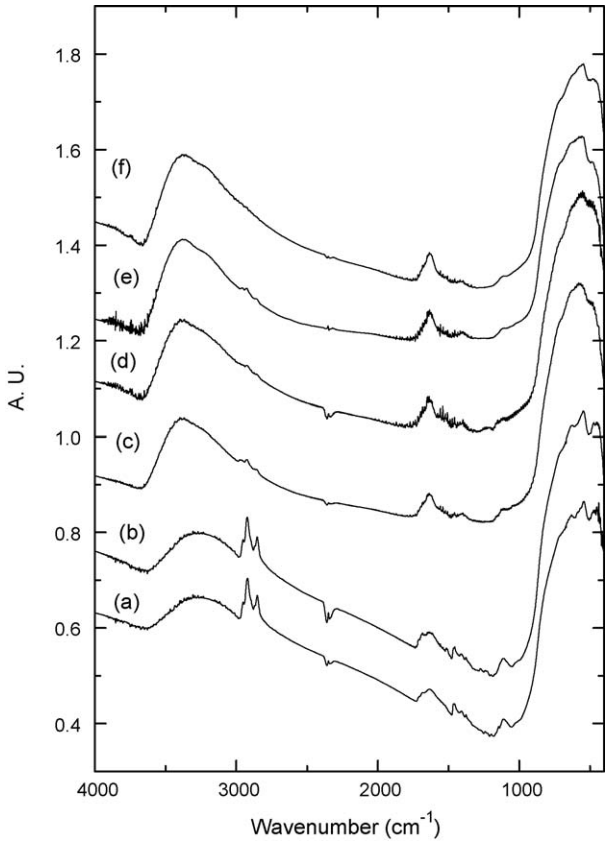

Fig. 8. The FTIR spectra of the used TOPO-capped TiO_2 (a) after first degradation of bisphenol A, (b) after first degradation of phenol, (c) after first degradation of bisphenol A and then washed with acetone, (d) after second degradation of bisphenol A and then washed with acetone, (e) after first degradation of phenol and then washed with acetone, and (f) after second degradation of phenol and then washed with acetone. The initial concentrations of the EDCs are 10 mg/l.

Fig. 9 shows the photocatalytic capability of the once-used TOPO-capped TiO_2 for degradation of 10 mg/l phenol and bisphenol A. To eliminate the interference from detached TOPO and intermediates left from the previous degradation, all the used catalysts were washed with acetone for 3 times. The used photocatalysts removed 0.3 and 3.2 mg/l of phenol and bisphenol A, respectively, from the solution in the dark. Compared to the high adsorptions of the fresh TOPO-capped TiO_2 (1.5 and 8.1 mg/l for phenol and bisphenol A, respectively), the detachment and partially decomposition of TOPO reduced the affinity of the modified TiO_2 toward the EDCs. However, the periods for 98% removal of the EDCs were shortened to 90–110 min. The enhanced apparent photocatalytic efficiencies were resulted from the remarkably increased specific surface area of the used photocatalysts (193 m^2/g). After normalizing the initial rates with the specific surface area, the used catalysts showed the intrinsic photocatalytic activities of 9.61×10^{-4} and 1.38×10^{-3} mg-g/l-min-m^2 for phenol and bisphenol A, respectively. The values, however, were 6.67×10^{-2} and 0.12 fold to the activities of the

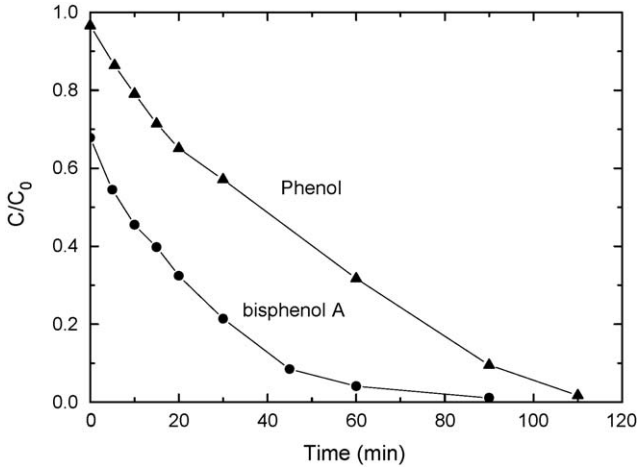

Fig. 9. The photocatalytic degradation of 10 mg/l (▲) phenol and (●) bisphenol A by the used TOPO-capped TiO_2.

fresh TOPO-capped TiO_2 for phenol and bisphenol A, respectively. These results clearly evidence that the covalently bonded surface modifier controls the high photocatalytic activity of TiO_2.

4. Conclusions

Results in this study clearly demonstrated that the TOPO-capped TiO_2 nanocrystals exhibited higher photocatalytic activity than P25 for decomposition of phenol and bisphenol A. The TOPO played the crucial role in the mechanisms and kinetics of the photocatalysis in the modified TiO_2 systems. The hydrophobic surface modifier inhibited the generation of hydroxyl radicals by preventing the attachment of water to TiO_2. Therefore, the photocatalysis in the modified TiO_2 system primarily underwent though partition followed by chemisorption and interfacial charge transfer between adsorbed compounds and the photocatalysts. On the other hand, the TOPO greatly enriched the EDCs on the surface of the modified TiO_2 by partition effect. In addition, it introduced substantial amounts of oxygenated radicals to facilitate chemisorptions and interfacial charge transfer. Partition and chemiadsorbability determined the degradation kinetics of the compounds having low and high log K_{ow} values, respectively. Relative to phenol, the TOPO-capped TiO_2 exhibited higher photocatalytic activity for decomposition of bisphenol A in their individual systems because of its high chemiadsorbability and direct photocatalytic tendency. In the competitive system, phenol was preferentially degraded because of its high degradable nature.

Acknowledgements

We thank the National Science Council, Taiwan, ROC (grant No. NSC97-2221-E-009-044-MY2) and MOE ATU Program for supporting this study financially.

Appendix A. Supplementary data

Supplementary data associated with this article can be found, in the online version, at doi:10.1016/j.apcatb.2009.06.035.

References

[1] W.V. Welshons, K.A. Thayer, B.M. Judy, J.A. Taylor, E.M. Curran, F.S. vom Saal, Environ. Health Perspect. 111 (2003) 994–1006.
[2] R. McKinlay, J.A. Plant, J.N.B. Bell, N. Voulvoulis, Environ. Int. 34 (2008) 168–183.
[3] S. Fukahori, H. Ichiura, T. Kitaoka, H. Tanaka, Environ. Sci. Technol. 37 (2003) 1048–1051.
[4] L. Liu, H.J. Liu, Y.P. Zhao, Y.Q. Wang, Y.Q. Duan, G.D. Gao, M. Ge, W. Chen, Environ. Sci. Technol. 42 (2008) 2342–2348.
[5] A.L. Linsebigler, G.Q. Lu, J.T. Yates, Chem. Rev. 95 (1995) 735–758.
[6] D.C. Hurum, K.A. Gray, T. Rajh, M.C. Thurnauer, J. Phys. Chem. B 109 (2005) 977–980.
[7] T.L. Thompson, J.T. Yates, Chem. Rev. 106 (2006) 4428–4453.
[8] A. Sclafani, J.M. Herrmann, J. Phys. Chem. 100 (1996) 13655–13661.
[9] K.V. Baiju, S. Shukla, K.S. Sandhya, J. James, K.G.K. Warrier, J. Phys. Chem. C 111 (2007) 7612–7622.
[10] M. Takeuchi, S. Dohshi, T. Eura, M. Anpo, J. Phys. Chem. B 107 (2003) 14278–14282.
[11] D.F. Watson, A. Marton, A.M. Stux, G.J. Meyer, J. Phys. Chem. B 108 (2004) 11680–11688.
[12] Y. Ou, J.D. Lin, H.M. Zou, D.W. Liao, J. Mol. Catal. A: Chem. 241 (2005) 59–64.
[13] O.V. Makarova, T. Rajh, M.C. Thurnauer, A. Martin, P.A. Kemme, D. Cropek, Environ. Sci. Technol. 34 (2000) 4797–4803.
[14] J.C. Yu, W.K. Ho, J.G. Yu, S.K. Hark, K. Iu, Langmuir 19 (2003) 3889–3896.
[15] G. Mele, R. Del Sole, G. Vasapollo, G. Marci, E. Garcia-Lopez, L. Palmisano, J.M. Coronado, M.D. Hernandez-Alonso, C. Malitesta, M.R. Guascito, J. Phys. Chem. B 109 (2005) 12347–12352.
[16] H. Park, W. Choi, J. Phys. Chem. B 109 (2005) 11667–11674.
[17] D. Cropek, P.A. Kemme, O.V. Makarova, L.X. Chen, T. Rajh, J. Phys. Chem. C 112 (2008) 8311–8318.
[18] S.M. Chang, R.A. Doong, J. Phys. Chem. B 110 (2006) 20808–20814.
[19] Z. Aksu, J. Yener, Process Biochem. 33 (1998) 649–655.
[20] C. Hansch, D. Hoekman, A. Leo, L.T. Zhang, P. Li, Toxicol. Lett. 79 (1995) 45–53.
[21] J.M. Coronado, A.J. Maira, J.C. Conesa, K.L. Yeung, V. Augugliaro, J. Soria, Langmuir 17 (2001) 5368–5374.
[22] D.C. Hurum, A.G. Agrios, K.A. Gray, T. Rajh, M.C. Thurnauer, J. Phys. Chem. B 107 (2003) 4545–4549.
[23] C.P. Kumar, N.O. Gopal, T.C. Wang, M.S. Wong, S.C. Ke, J. Phys. Chem. B 110 (2006) 5223–5229.
[24] K. Yang, Y. Dai, B. Huang, J. Phys. Chem. C 111 (2007) 18985–18994.
[25] R. Scotti, I.R. Bellobono, C. Canevali, C. Cannas, M. Catti, M. D'Arienzo, A. Musinu, S. Polizzi, M. Sommariva, A. Testino, F. Morazzoni, Chem. Mater. 20 (2008) 4051–4061.
[26] H. Yamashita, S. Kawasaki, Y. Ichihashi, M. Harada, M. Takeuchi, M. Anpo, G. Stewart, M.A. Fox, C. Louis, M. Che, J. Phys. Chem. B 102 (1998) 5870–5875.
[27] M. Janus, A.W. Morawski, Appl. Catal. B: Environ. 75 (2007) 118–123.
[28] G. Ramakrishna, H.N. Ghosh, Langmuir 19 (2003) 505–508.
[29] R. Comparelli, E. Fanizza, M.L. Curri, P.D. Cozzoli, G. Mascolo, R. Passino, A. Agostiano, Appl. Catal. B: Environ. 55 (2005) 81–91.
[30] S. Parra, J. Olivero, C. Pulgarin, Appl. Catal. B: Environ. 36 (2002) 75–85.
[31] C. Ooka, H. Yoshida, M. Horio, K. Suzuki, T. Hattori, Appl. Catal. B: Environ. 41 (2003) 313–321.